

> IEEE Transactions on Power Electronics <

A High-Efficiency Underwater Hybrid Wireless Power Transfer System with Low Plate Voltage Stresses

Xian Zhang, Guangyao Li, Ting Chen, *Member, IEEE*, Fengxian Wang, Qingxin Yang, and Weida Xu

Abstract—This paper proposes a high-efficiency underwater hybrid wireless power transfer (UHWPT) system with low plate voltage stresses to ensure a safe and stable power supply for underwater electrical equipment. The power transfer channel is constituted by an integrated magnetic-electric coupler, formed by nesting coils into C-shaped plates and integrating them into the LC-compensated topology. The system's working principle is analyzed in detail, providing the relationship among the circuit parameters, efficiency, and the same-side inter-plate (SIP) voltage. The impact of the geometric dimensions and insulation on electrical parameters is explored to provide a reference basis for designing the integrated magnetic-electric coupler. A system design method based on the double optimization parameters is hereby proposed. Then, an experimental prototype is set up to verify the feasibility of the design method. Experimental results show that the system achieves the load-independent constant current (CC) output with a maximum efficiency of 87.8%. Compared to the SS-compensated underwater inductive power transfer (UIPT) and capacitive power transfer (UCPT) systems at the same input power, the average suppression of the coil currents and the SIP voltage stresses of the proposed system is improved by 39.1% and 31.3%, respectively.

Index Terms—Underwater hybrid wireless power transfer (UHWPT), integrated magnetic-electric coupler, voltage stresses, constant current (CC).

I. INTRODUCTION

WITH the increasing demand for marine resource exploration, the imperative to enhance the core technological capabilities of underwater electrical equipment

This work was supported in part by the National Natural Science Foundation of China under Projects 52122701 and 52307009, in part by the Key Program of Natural Science Foundation of Tianjin 22JCZDJC00620, in part by the Hebei Provincial Central Guidance Local Science and Technology Development Project 236Z5201G, in part by the Colleges and Universities in Hebei Province Science and Technology Research Project CXY2024010 and in part by the Interdisciplinary Postgraduate Training Program of Hebei University of Technology HEBUT-Y-XKJC-2022109. (Corresponding author: Fengxian Wang.)

Xian Zhang, Guangyao Li, Ting Chen, Fengxian Wang and Weida Xu are with the State Key Laboratory of Reliability and Intelligence of Electrical Equipment, Hebei University of Technology, Tianjin 300401, China, and also with the Hebei Key Laboratory of Equipment and Technology Demonstration of Flexible DC Transmission, Hebei University of Technology, Tianjin 300401, China (e-mail: zhangxian@hebut.edu.cn; lgymecury@163.com; tingchen@hebut.edu.cn; fx-wang@outlook.com; 202131404038@stu.hebut.edu.cn).

Qingxin Yang is with the Tianjin University of Technology, Tianjin 300384, China (e-mail: qxyang@tjut.edu.cn).

becomes increasingly significant. Presently, underwater electrical equipment such as autonomous underwater vehicles (AUVs), remotely operated underwater vehicles (ROVs), and deep-sea submersibles face challenges, such as interface wear, leakage currents induced by wet plugging and unplugging, low reliability, and high maintenance costs [1-3]. These issues significantly impact the stability of power supply systems. Wireless power transfer (WPT) technology utilizes spatial electromagnetic transformation to achieve contactless energy transfer [4, 5], offering a solution to the aforementioned problems and proving highly suitable for powering underwater electrical equipment.

WPT in the underwater environment can be categorized into underwater inductive power transfer (UIPT) and underwater capacitive power transfer (UCPT) [6-8]. Unlike the IPT system in an air medium, the eddy current loss (ECL) caused by the coil currents in seawater can reduce system efficiency [6, 9]. To solve the ECL issue, Zhang et al. [10] proposed a coil structure with two transmitter coils and one receiver coil to reduce the ECL and designed a shared-compensated capacitance topology to enhance the robustness of the system against changing mutual inductance. However, this method requires additional transmitter coils, increasing the size and cost of the system. Yan et al. [11] developed an analytical model of eddy current loss for the UIPT system and found that the optimum operating frequency should be greater than the resonant frequency to achieve maximum dc-dc efficiency, but the improvement of system efficiency is low. The CPT system utilizes a high-frequency electric field for wireless power transfer [12, 13]. While the high voltage across the coupling plates is beneficial for extra power transfer capability, it increases the risk of dielectric breakdown and large leakage of electric field radiation [14, 15]. Especially in the high-conductivity seawater environment because the safety of the UCPT system is of significant importance. To solve the abovementioned issues, Luo et al. [16] maintained the voltage phase angle 90° across the capacitive coupler by designing compensation networks, thereby optimizing the voltage stresses across the coupler so that the coupling voltage can be fully utilized for power transfer. Lian et al. [17] realized the regulation of the plate voltage stresses by introducing the compensation element parameters into the plate voltage expression and proposed a parameter design method for a high-order double-sided *LCLC*-compensated CPT system that fulfills the predetermined plate voltage stresses to mitigate the air breakdown and electric field

> IEEE Transactions on Power Electronics <

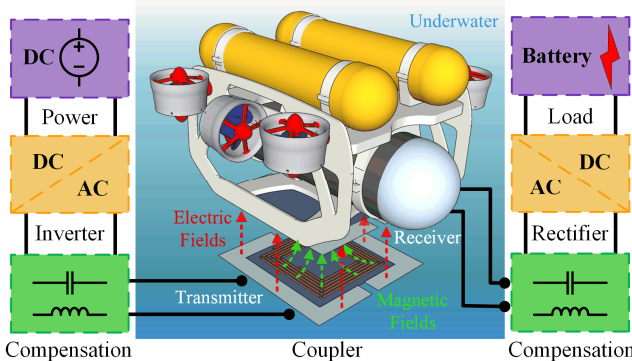


Fig. 1. Structure of the proposed UHWPT system.

radiation leakage. However, the aforementioned works all require high-order compensation networks to reduce the plate voltage stresses, which increases the system complexity.

As shown above, the UIPT and UCPT technologies exhibit distinct characteristics, while the transfer characteristics of both systems are susceptible to seawater. For example, the UIPT system offers high power density, safety, and strong applicability [6, 7], but it suffers from reduced system efficiency due to the ECL in seawater. In contrast, the UCPT system has a simple structure, low ECL, and longer transfer distance [18, 19], but the high conductivity of seawater increases the risk of dielectric breakdown. Meanwhile, in order to realize high-capacity power transfer, the magnetic field coupling energy transfer channel in the UIPT system needs to maintain a large coil current, and the electric field coupling energy transfer channel in the UCPT system needs to maintain a high voltage among the coupling plates.

The HWPT technology utilizes both electric and magnetic field coupling energy transfer channels for contactless power transfer [20]. It can reduce the ECL and coupling plates voltage stresses by allocating the power of the two types of transfer channels to ensure the system' efficient transfer and stable operation in underwater scenarios. The interaction of the two types of transfer channels can further improve the power transfer capability of the system [20]. Thus, the HWPT system is a superior alternative to the single UIPT and UCPT systems.

Studies have been carried out about the HWPT technology [20-24]. Lu et al. [21] proposed an *LC*-compensated HWPT system where the coils and plates of the coupler are arranged separately. The introduction of the capacitive coupler enhances the system's tolerance to misalignment. However, the separated arrangement increases the space occupation. Lu et al. [22] proposed a novel coupler for the HWPT system consisting of bending long strips of metal sheet integrated into the *LCL*-compensated topology, where the bent copper sheets have both coupling coils and capacitors characteristics. However, the overall size of the coupler is not ideally constrained. To reduce the overall size of the coupler, Luo et al. [20] designed an integrated coupler with the coils and plates arranged vertically. The research reveals that the system has high ant-misalignment performance, and the maximum output power variation is 8.3% with the coupler misalignment from 0 to 270 mm. However, the

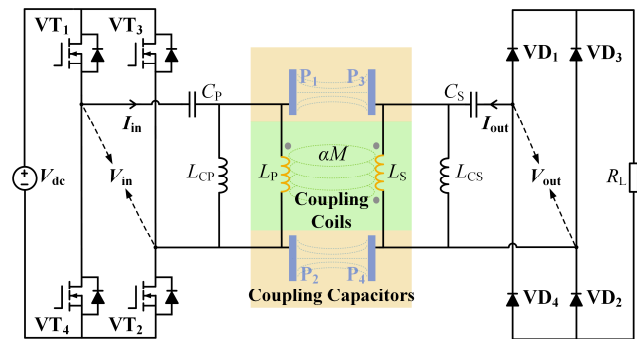


Fig. 2. Circuit topology of the *LC*-compensated UHWPT system.

vertical arrangement of the coils and plates results in the eddy current loss, decreasing the system transfer power and efficiency. In summary, the current research on HWPT predominantly focuses on the coupler structure design and enhancing misalignment tolerance, but there is a lack of research concerning the HWPT systems in the underwater environment.

In addressing the ECL in the UIPT system and the dielectric breakdown in the UCPT system, this paper proposes an underwater hybrid wireless power transfer (UHWPT) system. The main contributions are summarized as follows.

- 1) To facilitate both magnetic and electric field coupling energy transfer channels, an integrated magnetic-electric coupler suitable for the UHWPT system with a more compact structure is proposed.
- 2) The proposed *LC*-compensated UHWPT system is analyzed in detail, and the system adopts a design method based on the double optimization parameters, which filters out the optimal parameter range.
- 3) The HWPT technology can significantly reduce the ECL caused by the coil currents as well as the voltage stresses among the coupling plates by rationally allocating the power of the two types of transfer channels, providing a novel and adaptable solution for efficient and safe underwater wireless power transfer.

The rest of this article is organized as follows. Section II introduces the system structure and analyzes the working principle in detail. Section III analyzes the influence of the geometric dimensions and insulation on the coupler parameters. Section IV proposes a design method for the system based on the double optimization parameters. Section V establishes an experimental prototype to verify the feasibility of the design method. Finally, conclusions are drawn in Section VI.

II. SYSTEM STRUCTURE AND WORKING PRINCIPLE

A. UHWPT System Structure

The structure of the proposed UHWPT system applied to underwater electrical equipment is shown in Fig. 1. The corresponding circuit topology is depicted in Fig. 2. On the transmitter side, a full-bridge inverter is employed to supply high-frequency AC power to the system. On the receiver side,

> IEEE Transactions on Power Electronics <

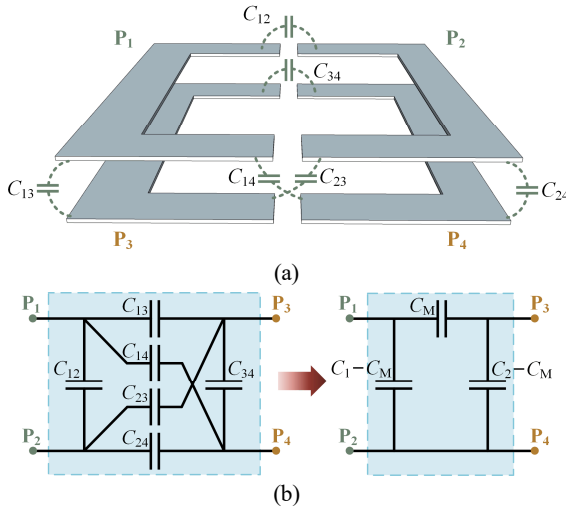


Fig. 3. (a) The four plates structure. (b) Circuit model of the plates.

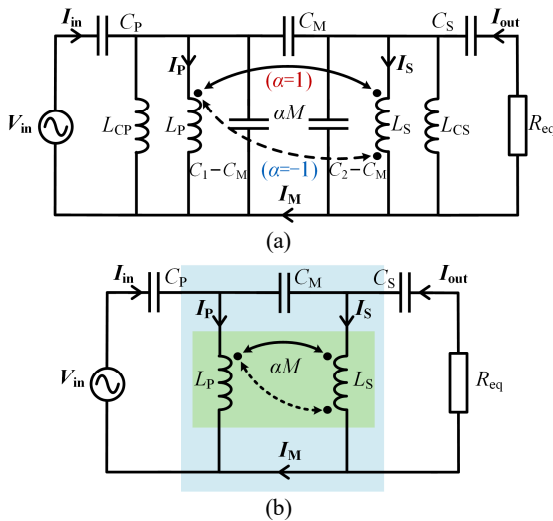


Fig. 4. Equivalent circuit model of the proposed UHWPT system. (a) LC-compensated topology. (b) Simplified SS-compensated topology.

a full-bridge diode rectifier provides DC power to the load resistance R_L . The coupling coils and capacitors serve as the transfer channel of magnetic field coupling energy and electric field coupling energy, respectively. The system employs the *LC*-compensated topology, where L_{CP} and L_{CS} are compensation inductors, and C_P and C_S are compensation capacitors. The high voltage imposed on the IPT coils in this topology can be fully utilized as the driving voltage of the CPT coupler to build a UHWPT system that can transmit both magnetic and electric field coupling energy, extending the transfer channel, and improving the power transfer capability. As shown in Fig. 2, there is mutual inductance M between the coupling coils. The variable α (either 1 or -1) is defined as the coils' connection to characterize the coupling polarity of L_P and L_S , where $\alpha = 1$ represents the positive connection and $\alpha = -1$ represents the reverse connection.

The rational design of the coupler is crucial for achieving hybrid coupling energy transfer. As shown in Fig. 1, this paper proposes an integrated magnetic-electric coupler composed of

nesting coils and C-type plates. The ferrites are adhered to the back of the coils to reduce ECL in the underwater environment and enhance the magnetic coupling strength. Utilizing the fringe effect of parallel plate capacitors [25], the C-type plates are adopted to ensure the compactness of the coupler and to reduce the eddy currents on the plate under the premise of small changes in the coupling capacitance. The coupler parameters will be analyzed in detail in Section III.

B. Circuit Working Principle

For the coupling capacitors, the four plates are arranged as shown in Fig. 3(a), where plates P₁ and P₂ work as the transmitter, and P₃ and P₄ work as the receiver. The distributed capacitances among the four plates can be represented using a six-capacitor model in Fig. 3(b). C₁₃ and C₂₄ are the main coupling capacitances of P₁ to P₃ and P₂ to P₄, while C₁₂ and C₃₄ are the leakage capacitances of P₁ to P₂ and P₃ to P₄, and C₁₄ and C₂₃ are the cross-coupling capacitances of P₁ to P₄ and P₂ to P₃. According to Zhang et al. [26], the six-capacitor model can be simplified to a π shape model. In Fig. 3(b), C₁ and C₂ represent self-capacitance on the transmitter side and receiver side, respectively, and C_M represents mutual capacitance. The capacitances C₁, C₂, and C_M are defined as

$$\begin{cases} C_1 = C_{12} + \frac{(C_{13} + C_{14})(C_{23} + C_{24})}{C_{13} + C_{14} + C_{23} + C_{24}} \\ C_2 = C_{34} + \frac{(C_{13} + C_{23})(C_{14} + C_{24})}{C_{13} + C_{14} + C_{23} + C_{24}}, \\ C_M = \frac{C_{13}C_{24} - C_{14}C_{23}}{C_{13} + C_{14} + C_{23} + C_{24}} \end{cases}, \quad (1)$$

Using the fundamental harmonic approximation (FHA) method and π shape model of coupling capacitors, the equivalent circuit of the *LC*-compensated UHWPT system can be simplified as Fig. 4(a), where V_{in} is the input voltage and $R_{eq} = 8R_L/\pi^2$ is the equivalent resistance observed before the rectifier. I_{in} and I_{out} denote the input and output currents. I_M , I_P , and I_S are the currents flowing through the mutual capacitance (C_M), the transmitter coils (L_P), and the receiver coils (L_S), respectively. L_{CP} and L_{CS} serve as compensation inductors to resonate with the equivalent capacitance $C_1 - C_M$ and $C_2 - C_M$, respectively, to compensate for the reactive power between the plates. The resonance conditions satisfy

$$\begin{cases} \omega(C_1 - C_M) = \frac{1}{\omega L_{CP}} \\ \omega(C_2 - C_M) = \frac{1}{\omega L_{CS}} \end{cases}, \quad (2)$$

where ω is the operating angular frequency of the system.

When (2) is satisfied, the *LC*-compensated topology can be further simplified into an SS-compensated topology, as shown in Fig. 4(b). According to Kirchhoff's Voltage and Current Laws, the circuit equations can be expressed as

> IEEE Transactions on Power Electronics <

$$\begin{cases} \frac{1}{j\omega C_p} I_{in} + j\omega L_p I_p + j\omega \alpha M I_s = V_{in} \\ j\omega L_p I_p + j\omega \alpha M I_s = \frac{1}{j\omega C_M} I_M + j\omega L_s I_s + j\omega \alpha M I_p \\ j\omega L_s I_s + j\omega \alpha M I_p = -\frac{1}{j\omega C_s} I_{out} - R_{eq} I_{out} \\ I_p + I_M = I_{in} \\ I_M + I_{out} = I_s \end{cases} \quad (3)$$

Based on (3), The system's output current I_{out} can be calculated as

$$I_{out} = \frac{X_1}{X_2 R_{eq} + j X_3} V_{in}, \quad (4)$$

where X_1-X_3 are defined as (5), shown at the bottom of the next page. To achieve the load-independent constant current (CC) output, it is necessary to satisfy

$$X_2 = 0 \Rightarrow I_{out} = -j \frac{X_1}{X_3} V_{in}. \quad (6)$$

The system's input current I_{in} can be calculated as

$$I_{in} = \frac{j X_6 + X_7}{j X_4 + X_5} V_{in}, \quad (7)$$

where X_4-X_7 is defined as (8), shown at the bottom of the page. To ensure efficient energy transfer in the system, the Zero Phase Angle (ZPA) input is required, which can be expressed as

$$\text{Im}(Z_{in}) = \text{Im}\left(\frac{V_{in}}{I_{in}}\right) = \text{Im}\left(\frac{j X_4 + X_5}{j X_6 + X_7}\right) = 0. \quad (9)$$

By combining (6) and (9), the resonance condition for input ZPA and CC output can be expressed as

$$\begin{cases} \omega C_p = \frac{\omega^2 C_M (L_p + L_s - 2\alpha M) - 1}{\omega (\omega^2 C_M L_p L_s - \omega^2 C_M M^2 - L_p)} \\ \omega C_s = \frac{\omega^2 C_M (L_p + L_s - 2\alpha M) - 1}{\omega (\omega^2 C_M L_p L_s - \omega^2 C_M M^2 - L_s)} \end{cases} \quad (10)$$

According to the principles of inductive and capacitive power transfer, the inductive power P_M and the capacitive power P_E can be respectively expressed as

$$\begin{aligned} P_M &= \text{Re}(j\omega \alpha M I_p \cdot (-I_s)^*) \\ &= \frac{(1 + (2\alpha M - L_p - L_s) C_M \omega^2)^2 2\alpha M R_{eq} V_{in}^2}{(C_M (M^2 - L_p L_s) \omega^2 + \alpha M)^3 \omega^2} \end{aligned} \quad (11)$$

$$\begin{cases} X_1 = C_s C_p \omega^3 (\alpha M + C_M M^2 \omega^2 - C_M L_p L_s \omega^2) \\ X_2 = \left((L_p L_s - M^2) C_M C_p \omega^4 + (2\alpha M - L_p - L_s) \right) \omega C_s \\ X_3 = \left((L_p + L_s - 2\alpha M) C_M \omega^2 + (L_p C_p + L_s C_s) \omega^2 + \right) \\ \left. \left((M^2 - L_p L_s) (C_p C_s + C_M C_p + C_M C_s) \omega^4 - 1 \right) \right. \end{cases} \quad (5)$$

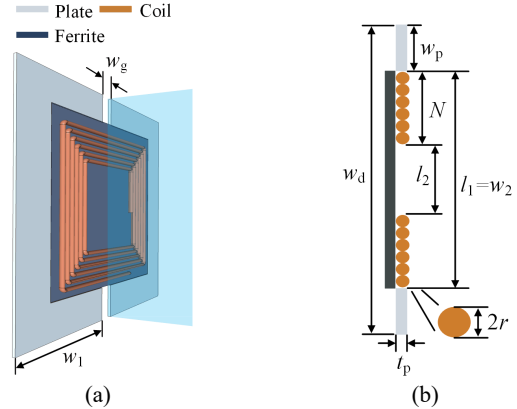


Fig. 5. The structure and dimension of the coupler. (a) 3-D view. (b) longitudinal section view.

$$\begin{aligned} P_E &= \text{Re}((j\omega L_p I_p + j\omega M I_s) I_M^*) \\ &= \frac{(1 + (2\alpha M - L_p - L_s) C_M \omega^2)^2}{(C_M (M^2 - L_p L_s) \omega^2 + \alpha M)^3} \\ &\quad \cdot \frac{(L_p L_s - M^2) 2 C_M R_{eq} V_{in}^2}{(C_M (M^2 - L_p L_s) \omega^2 + \alpha M)}, \end{aligned} \quad (12)$$

Based on (11) and (12), the power ratio β between the capacitive power and inductive power can be defined as

$$\beta = \frac{P_E}{P_M} = \frac{C_M (M^2 - L_p L_s) \omega^2}{\alpha M} = \frac{C_M \sqrt{L_p L_s} (k_M^2 - 1) \omega^2}{\alpha k_M}, \quad (13)$$

where k_M is the magnetic field coupling coefficient, which can be expressed as

$$k_M = \frac{M}{\sqrt{L_p L_s}}. \quad (14)$$

It can be observed from (13) that β is related to coupler parameters, ω , and α . It's worth noting that the coils' connection directly affects the directions of the inductive and capacitive power transfer. If $\alpha = 1$, $\beta < 0$, indicating that the two types of power are transmitted in opposite directions. Conversely, if $\alpha = -1$, $\beta > 0$, the two types of power transfer are transmitted in the same directions. As a result of the above discussion, the coils' connection is chosen to be $\alpha = -1$ to ensure that the system's transfer power is an addition of the inductive power with the capacitive power.

$$\begin{cases} X_4 = \left((L_p L_s - M^2) C_M C_p \omega^4 + (2M - L_p - L_s) C_M \omega^2 \right) C_s R_{eq} \omega \\ X_5 = \left(C_M C_p + C_M C_s + C_p C_s \right) (L_p L_s - M^2) \omega^4 + (2M - L_p - L_s) \\ C_M \omega^2 - (C_p L_p + C_s L_s) \omega^2 + 1 \\ X_6 = \left((L_p L_s - M^2) C_M C_s \omega^4 + (2M - L_p - L_s) C_M \omega^2 \right) C_p \omega \\ X_7 = \left((L_p + L_s - 2M) C_M \omega^2 - 1 \right) C_p C_s R_{eq} \omega^2 \end{cases} \quad (8)$$

> IEEE Transactions on Power Electronics <

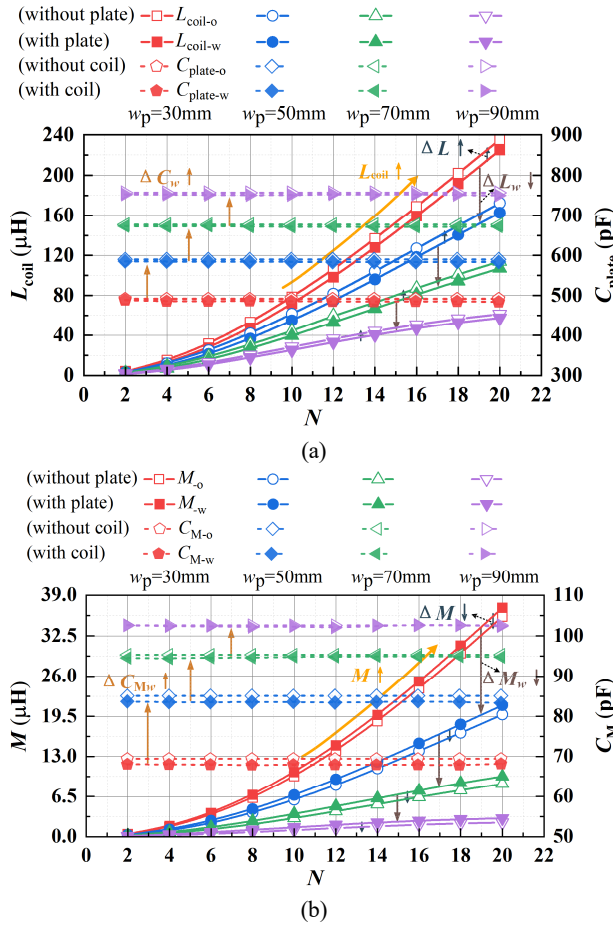


Fig. 6. Effect of geometric dimensions on the electrical parameters of the coupler. (a) Inductance. (b) Capacitance.

III. COUPLER PARAMETER ANALYSIS

A. Proposed Integrated Magnetic-electric Coupler

As shown in Fig. 5, the proposed integrated magnetic-electric coupler consists of two parts: the coupling coils and coupling capacitors. The coupler is symmetric with respect to the transmitter and receiver sides. The coupling coils are made of tightly wound high-frequency Litz wire with a radius of r , where the number of coil turns is N , and the outer edge length of the coil is l_1 . The inner edge length of the coil l_2 satisfies $l_2 = l_1 - 4r$. The coupling capacitors are made of four aluminum plates, with w_d , w_1 , w_p being the outer edge length, outer edge width and inner width of the plate, respectively. In addition, w_g is the gap between the outer edges of parallel plates on the same side, and $t_p = 2\text{ mm}$ is the plate thickness. The outer edge width of the plate, w_1 , is such that $w_1 = (w_d - w_g)/2$, and the inner edge length of the plate, w_2 , fulfills $w_2 = l_1 = w_d - 2w_p$. The transfer distance of the coupler is d .

B. Coupler Parameters: Impact of Geometric Dimensions

According to the definition of the inner edge length of plate w_2 , there is a constraint relationship between the spatial structure of the coupling coils and capacitors. Besides, the dimensions of both parts will affect the electrical parameters of the coupler. The

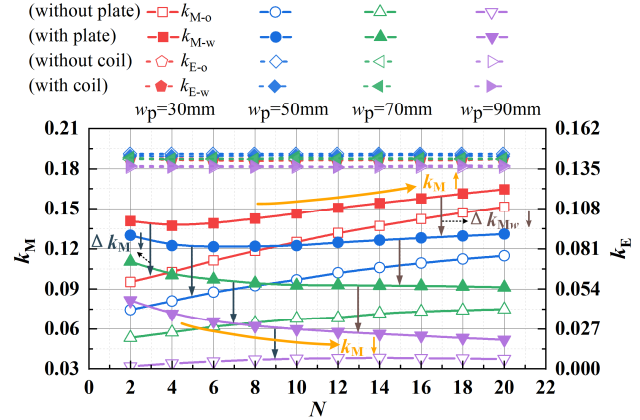


Fig. 7. Effect of geometric dimensions on the coupling coefficient.

selection of sizes for the plates and coils needs to consider the impact on the power ratio between the two types of coupling energy transfer channels as well as the ECL caused by the coil currents. This section primarily focuses on the influence of geometric dimensions on the electrical parameters of the coupler.

In this design, the overall dimensions of the coupler are fixed at $300 \times 300\text{ mm}$. With w_d set to 300 mm , w_g set to 10 mm , and d set to 120 mm , the variation of the electrical parameters of the coupler with the coil turns N for different the inner width of the plate w_p is analyzed. $L_{\text{coil-o}}$ is the self-inductance of the coil without considering the influence of the plates, and $L_{\text{coil-w}}$ is the self-inductance of the coil considering the influence of the plates. A comparison of the two self-inductances characterizes the effect of the plate on the coupling coils. $C_{\text{plate-o}}$ is the self-capacitance of the plate without considering the influence of the coils, and $C_{\text{plate-w}}$ is the self-capacitance of the plate considering the influence of the coils. The variation of $L_{\text{coil-o}}$, $L_{\text{coil-w}}$, $C_{\text{plate-o}}$, and $C_{\text{plate-w}}$ with the number of coil turns for four different inner widths of the plate ($w_p = 30, 50, 70, 90\text{ mm}$) is shown in Fig. 6(a). The self-inductance is influenced by both N and w_p , as the increase in N leads to higher self-inductance, while the increase in w_p leads to lower self-inductance. The impact of the coils on self-capacitance can be neglected, and the self-capacitance is primarily influenced by w_p , increasing with w_p . In addition, due to the eddy current effect of the metal, $L_{\text{coil-o}}$ is larger than $L_{\text{coil-w}}$, indicating that the integrated plates affect the self-inductance.

The variations of M_o , M_w , $C_{\text{plate-o}}$, and $C_{\text{plate-w}}$ with the number of coil turns for different inner widths of the plate w_p are shown in Fig. 6(b). It can be observed that the variations in mutual inductance and mutual capacitance align with the trends in self-inductance and self-capacitance. The difference is that M_o is smaller than M_w because grooved or perforated aluminum plates create an additional electromagnetic field that enhances the main magnetic flux of the system [27].

The ferrites attached to the back of the coils, along with the C-type plates affixed on the outer surface of the coils in the integrated magnetic-electric coupler serve a dual purpose. They provide the shielding to reduce electromagnetic exposure and enhance the magnetic coupling by promoting the magnetizing effect. To assess the coupling performance and leakage shielding performance of the WPT system, the magnetic field coupling

> IEEE Transactions on Power Electronics <

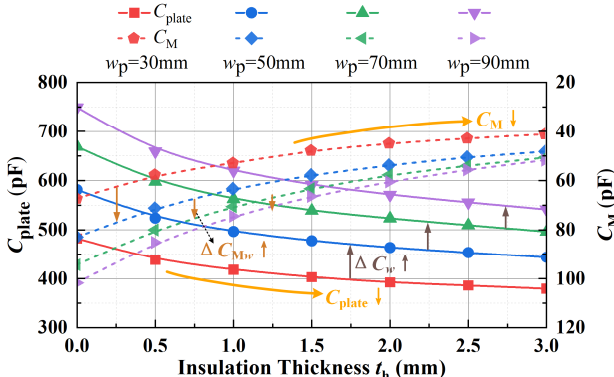


Fig. 8. Effect of insulation thickness on the capacitance.

coefficient k_M and the electric field coupling coefficient k_E are introduced, where the electric field coupling coefficient can be expressed as

$$k_E = \frac{C_M}{C_{plate}}. \quad (15)$$

Fig. 7 shows the variation of k_{M-o} , k_{M-w} , k_{E-o} , and k_{E-w} with the number of coil turns for different inner widths of the plate w_p . k_{M-o} increases with the number of coil turns, and its growth trend is faster when w_p is smaller. The variation trend of k_{M-w} is also related to w_p . When $w_p = 70$ mm and 90 mm, k_{M-w} decreases with coil turns. When $w_p = 30$ mm and 50 mm, k_{M-w} increases with coil turns. In contrast, k_{E-o} and k_{E-w} are hardly affected by N and w_p and remain around 0.14. Due to the enhancement of main magnetic flux by the C-type plates, k_{M-w} is greater than k_{M-o} . Note that the k_M of the integrated magnetic-electric coupler is significantly enhanced compared to the single coupler with the same coupling coils' dimensions, which improves the magnetic coupling performance of the system.

C. Coupler Parameters: Impact of Insulation

To make the designed coupler suitable for the underwater environment, the surface of the coupler is covered by epoxy resin as the insulation layer with a relative permittivity of 5. Based on the analysis in the previous section, the effect of the coils on the capacitance of the plate can be neglected. The capacitance is affected by the relative permittivity of the medium, so the introduction of the insulation layer changes the capacitance of the plate.

Fig. 8 shows the variation of the self-capacitance C_{plate} and mutual capacitance C_M with the insulation thickness t_h for different inner widths of the plate w_p . It can be found that C_{plate} and C_M decrease with the insulation thickness t_h , and its decreasing trend is faster when w_p is larger. It is worth noting that C_M decreases with different degrees of intensity as t_h increases at different w_p . When insulation thickness t_h increases from 0 to 3 mm, C_M ($w_p = 30$ mm) and C_M ($w_p = 50$ mm) decrease by 38.9% and 41.8%, respectively, while C_M ($w_p = 70$ mm) and C_M ($w_p = 90$ mm) decrease by 46.3% and 49.1%, respectively. It shows that the larger the opposing surface area of the plates, the higher the sensitivity of the mutual capacitance to the insulation thickness. Considering that the increase in the insulation thickness t_h will sharply reduce the mutual capacitance C_M . In this paper, the insulation thickness t_h is set to be 0.5 mm.

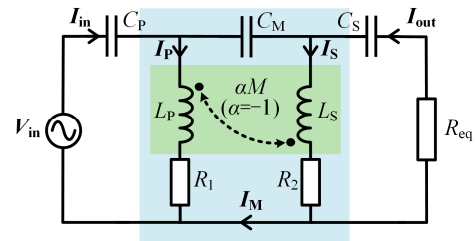


Fig. 9. Equivalent circuit of the UHWPT system considering the ECL.

IV. SYSTEM DESIGN AND SIMULATION

A. Double Optimization Parameters

According to the analysis of the power ratio in Section II-B, and the influence of the geometric dimensions and insulation on the electrical parameters of the coupler in Section III, this section proposes a design method for the underwater HWPT system based on the double optimization parameters to achieve higher system efficiency and lower plate voltage stresses.

For the WPT system operating in seawater, the ECL on the system efficiency needs to be considered. Fig. 9 shows the equivalent circuit of the UHWPT system considering the ECL. To simplify the analysis, it is assumed that both sides of the coupler are entirely symmetrical, i.e., $L = L_P = L_S$ and $R = R_1 = R_2$. In this case, $R_1 = R_P + R_{eddy}$, $R_2 = R_S + R_{eddy}$, where R_P and R_S represent the internal resistances of the coils, and R_{eddy} represents the additional equivalent resistances of the coils resulting from the ECL. According to [28], R_{eddy} can be expressed as

$$R_{eddy} = \omega \mu N^2 \int_{r_1}^{r_2} r dr \int_{r_1}^{r_2} \rho d\rho \int_0^\pi e^{-\sqrt{\frac{\omega \mu \gamma}{2}} s} \sin \sqrt{\frac{\omega \mu \gamma}{2}} s \cos \varphi d\varphi, \quad (16)$$

where μ is permeability, γ is conductivity, r_1 is the inner radius of the coil, and r_2 is the outer radius of the coil.

Defining the coil quality factor $Q = \omega L/R$, substituting the resonance condition (10), and neglecting the high-order terms, the system efficiency can be expressed as

$$\eta = \frac{P_{out}}{P_{in}} \approx \frac{\omega L Q^3 (1+\beta)^2 (2\beta k_M - 1) R_{eq}}{(7\beta k_M - 1)(6\beta k_M - 1)(3\beta k_M - 1)(\omega L + QR_{eq})^2}. \quad (17)$$

The high-conductivity seawater environment exacerbates the risk of the breakdown. Optimization of plate voltage stresses is required to ensure the system's safe operation. The risk of the opposite-side inter-plate (OIP) breakdown can be neglected for the transfer distance set in this article. Therefore, the analysis in this section focuses on the ability of the proposed UHWPT system to suppress the same-side inter-plate (SIP) voltage stresses. In order to characterize the ability of the proposed system to suppress the SIP voltage stresses compared to the SS-compensated UCPT system, the voltage suppression coefficient can be defined as $\lambda = |V_{p-UCPT}|/|V_{p-UHWPT}|$, where V_{p-UCPT} and $V_{p-UHWPT}$ denote the SIP voltage of the UCPT and UHWPT systems, respectively. With $C = C_1 - C_M = C_2 - C_M$, the magnitude of the SIP voltage in the SS-compensated UCPT

> IEEE Transactions on Power Electronics <

system can be expressed as

$$\begin{aligned} |V_{P-UCPT}| &= \left| \frac{\mathbf{I}_P}{j\omega(C_1 - C_M)} \right| = \left| \frac{\mathbf{I}_P}{j\omega C} \right| \\ &= \left| \frac{(2C\omega R_{eq} + j)C_M^2 + 3C^2 C_M \omega R_{eq} + C^3 \omega R_{eq}}{jC_M^2} \right| V_{in} \\ &= \left| (1 - 2jC\omega R_{eq}) + \frac{(3C_M + C)C^2 \omega R_{eq}}{jC_M^2} \right| V_{in}. \end{aligned} \quad (18)$$

The magnitude of the SIP voltage in the *LC*-compensated UHWPT system can be expressed as

$$\begin{aligned} |V_{P-UHWPT}| &= |\omega L_p \mathbf{I}_P + j\omega M \mathbf{I}_S| \\ &= \left| \frac{C_M A \omega^3 - 2jABR_{eq} - 2AM\omega + j(2BL - A)R_{eq} + M^2\omega - jLR_{eq}}{\omega(A - M)^2} \right| V_{in} \\ &= \left| \frac{(AC_M\omega^2 - 2AM + M^2)\omega - j(2AB - 2BL + A + L)R_{eq}}{(A - M)^2\omega} \right| V_{in}, \end{aligned} \quad (19)$$

where A and B are defined as

$$\begin{cases} A = (M^2 - L^2)C_M\omega^2 \\ B = (M + L)C_M\omega^2 \end{cases}. \quad (20)$$

To realize the high-efficiency UHWPT with low plate voltage stresses, this section introduces two optimization parameters (η , λ) as metrics to evaluate the system efficiency and suppression capability of the plate voltage stresses. These optimized parameters are applied to the design of the integrated magnetic-electric coupler.

B. Parameter Design and Simulation

The proposed system in this paper aims to address the issues of reduced efficiency due to the ECL in seawater and the safety concerns related to plate voltage stresses. The tradeoff between the low plate voltage stresses and high system efficiency should be considered in the system design. Based on the dual optimization parameters for the UHWPT system outlined in Section IV-A, the process of optimized system parameter design is shown in Fig. 10.

The input voltage and load resistance are given according to the required application. Usually, the working frequency of the IPT system is several tens kHz, while that of the CPT system is several MHz. For the HWPT system, both types of transfer channels share the working frequency. According to (13), lower working frequency leads to a sharp rise in the percentage of the inductive power, increasing eddy current loss caused by the coil currents, which is not conducive to efficiency optimization. In comparison, higher working frequency leads to a sharp rise in the percentage of the capacitive power, increasing plate voltage and exacerbating electric field radiation. Meanwhile, the switching loss of the inverter at a higher frequency will further reduce system efficiency. Based on the above discussion and previous studies of the HWPT system, the working frequency of the proposed system is set to be 800 kHz. Besides, the plate dimensions and transfer distance can be determined by the underwater application. To simplify the integrated magnetic-

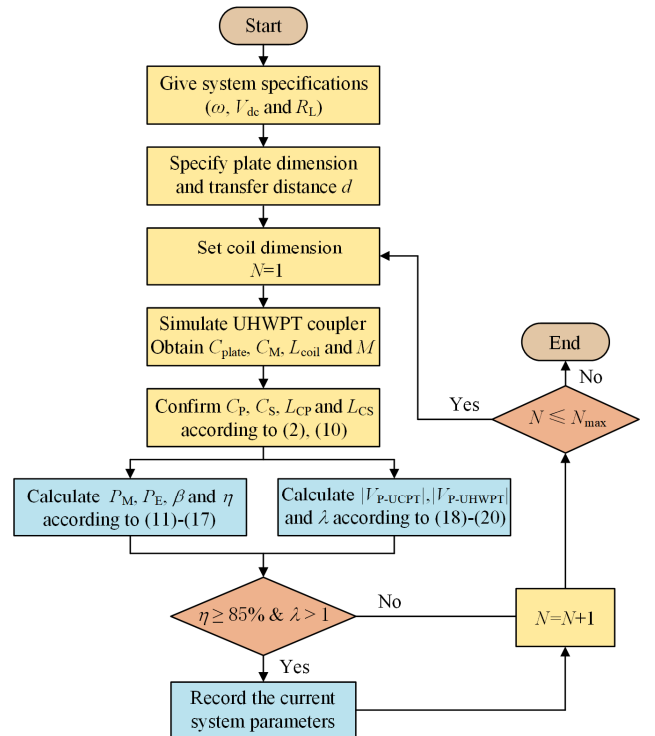


Fig. 10. The design process of the proposed system.

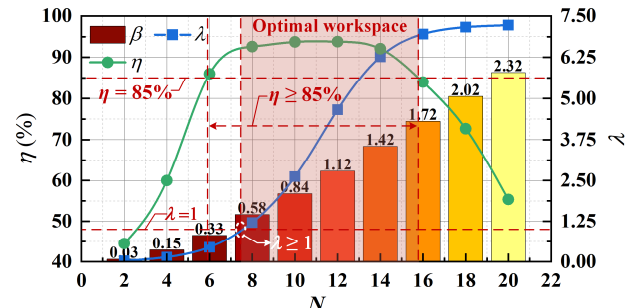


Fig. 11. The power ratio, efficiency, and voltage suppression factor versus coil turns N .

electric coupler design, the coil turns N are taken as the design object. The field-circuit coupling model is constructed to obtain C , C_M , L , and M under different coil turns. According to (2) and (10), the compensation parameters are determined. Then, the system efficiency and voltage suppression coefficient can be calculated based on (11)–(17) and (18)–(20), respectively. The system parameters that meet the conditions $\eta \geq 85\%$ and $\lambda > 1$ are obtained by iterating through coil turns ($N \leq N_{max}$). The purpose of setting $\eta \geq 85\%$ is to fulfill the need for system efficiency in underwater scenarios, and the purpose of setting $\lambda > 1$ is to ensure that the SIP voltage of the proposed system is less than that of the UCPT system.

Based on the discussion in Section III, the plate dimensions can be determined. w_d is set to be 300 mm, and w_g is set to be 10 mm. w_p is set to be 50 mm due to the better coupling performance of the system at this point, and the transfer distance d is set to be 120 mm. Following the underwater

> IEEE Transactions on Power Electronics <

TABLE I
SYSTEM SPECIFICATIONS AND CIRCUIT PARAMETERS

Parameter	Value	Parameter	Value
w_d	300 mm	w_g	10 mm
w_p	50 mm	l_1	200 mm
d	120 mm	N	8
f	800 kHz	V_{dc}	100 V
L_P	36.8 μ H	L_S	37.2 μ H
C_1	531.5 pF	C_2	525.3 pF
M	4.3 μ H	C_M	72.6 pF
L_{CS}	86.2 μ H	L_{CP}	87.4 μ H
C_P	977.6 pF	C_S	968.2 pF
R_1	1.67 Ω	R_2	1.69 Ω

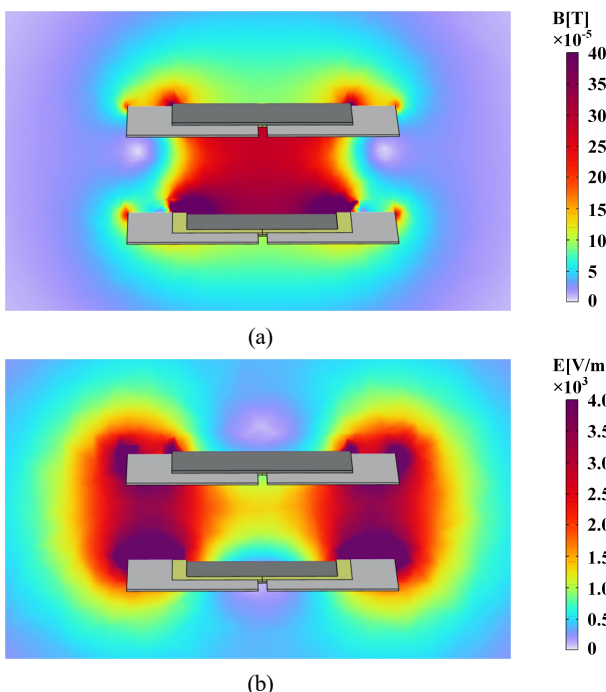


Fig. 12. Fields distribution of the coupler. (a) Magnetic field distribution. (b) Electric field distribution.

HWPT system design method in this section, Fig. 11 illustrates the variation trends of the power ratio, efficiency, and voltage suppression factor as a function of the number of coil turns. As N increases from 2 to 20, β increases from 0.04 to 2.57, which is because the growth rate of self-inductance is higher than the growth rate of k_E , improving the percentage of capacitive power according to (13). Therefore, when $N \leq 12$, η increases with N , indicating that the increase in the power ratio improves the system efficiency. Conversely, when $N \geq 12$, η decreases as N increases. This is because the increase in N leads to a sharp rise in R_{eddy} based on (16), resulting in a decrease in the system efficiency, while λ is positively correlated with N . According to the optimization conditions, the coil turns can vary within the $8 \leq N \leq 15$ range. In this range, the system efficiency remains at 85% or higher, and the proposed system is reduced in terms

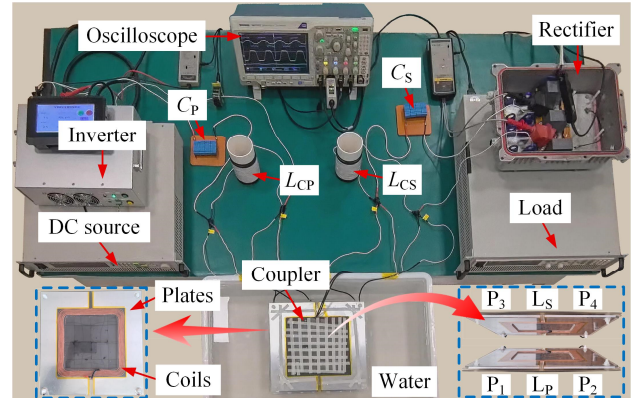


Fig. 13 Experimental prototype of the UHWPT system.

of the SIP voltage stresses compared to the SS-compensated UCPT system. To verify the feasibility of the proposed design method, coil turns are taken as $N = 8$. Table I lists the system specifications and circuit parameters.

The magnetic field distribution of the coupler is shown in Fig. 12(a), where the magnetic flux is primarily confined between the transmitter and receiver coils due to the shielding effects of the ferrite and the plates. The electric field distribution of the coupler is shown in Fig. 12(b), with a safety limit of 614 V/m according to the IEEE C95.1 standard [16]. Therefore, the safe range is 150 mm away from the coupler.

V. EXPERIMENT

A. Experimental Setup

An experiment prototype is constructed to verify the proposed UHWPT system, which is shown in Fig. 13. The system specifications and the circuit parameters are specified in Table I. The coils and compensation inductors are fabricated by 660-strand Litz-wire, which are wound around PVC pipes to mitigate high-frequency loss. Aluminum plates are employed to construct the capacitor coupler, where the dimensions of the transmitter plates P_1 and P_2 are the same as the receiver plates P_3 and P_4 . The compensation capacitors C_P and C_S employ high-frequency thin-film capacitors from KEMET with a maximum peak AC voltage rating of 700 V and an actual capacitance tolerance of $\pm 5\%$. The coupler is positioned within a seawater environment and requires insulation and waterproofing. The designed coils and plates are fixed to 2 mm-thick acrylic boards, with iron oxide material affixed to the back. In order to realize the insulation isolation between the same side plates and coils, the two parts need to leave a gap to avoid voltage breakdown. In addition, the plate edges are insulated and voltage-treated with high-voltage insulation tapes to prevent electrical leakage from sharp edges. The surface of the coupler is coated with a waterproof clear epoxy resin to ensure reliable insulation.

Since the switching frequency is 800 kHz, wide bandgap devices SiC MOSFETs (C3M0075120D) are employed in the inverter to provide high-frequency AC excitation, and SiC diodes are used in the rectifier. The digital controller (TMS320F28335) is employed to generate pulse-width modulation (PWM) signals for SiC MOSFETs to adjust the

> IEEE Transactions on Power Electronics <

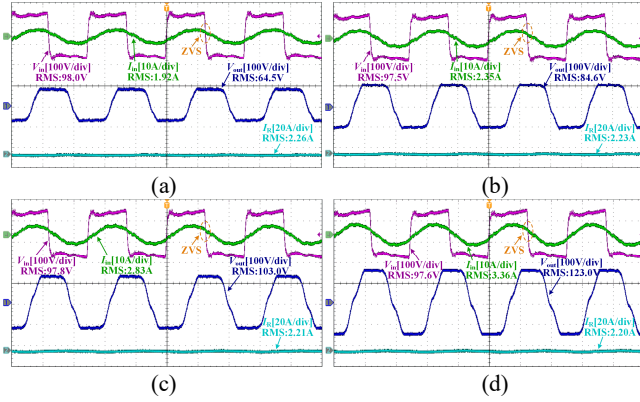


Fig. 14. Experimental waveforms of the inverter and load (a) $R_L = 30 \Omega$ (b) $R_L = 40 \Omega$ (c) $R_L = 50 \Omega$ (d) $R_L = 60 \Omega$.

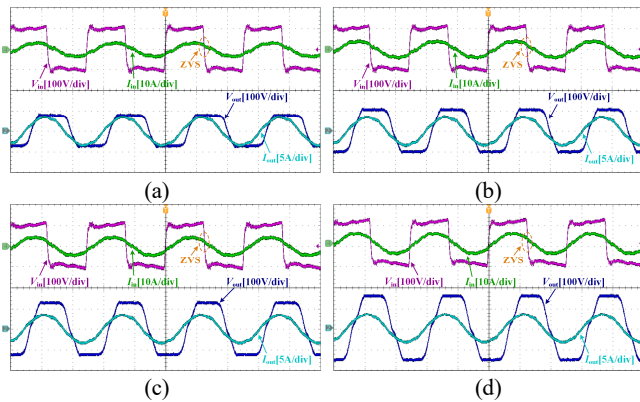


Fig. 15. Experimental input and output waveforms (a) $R_L = 30 \Omega$ (b) $R_L = 40 \Omega$ (c) $R_L = 50 \Omega$ (d) $R_L = 60 \Omega$.

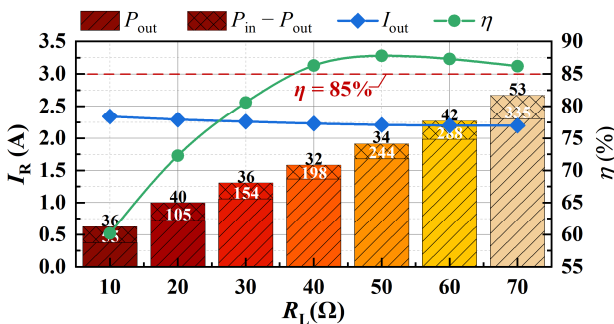


Fig. 16. The load current, efficiency, and power with different load resistance.

switching frequency.

B. Experimental Results

Fig. 14 shows the experimental waveforms of the inverter and load under different resistances. It indicates that the input voltage V_{in} and current I_{in} are almost in phase when the load varies from 30 to 60 Ω in Fig. 14(a) to (d). To reduce switching loss and ensure stable and safe operation of the inverter, it is necessary to realize the ZVS of the MOSFETs, so that the phase of I_{in} is slightly lagging the phase of V_{in} based on the near-ZPA input. Meanwhile, as shown in Fig. 15, the input voltage V_{in} leads the output voltage I_{out} nearly by 90°, which matches the analysis in (6).

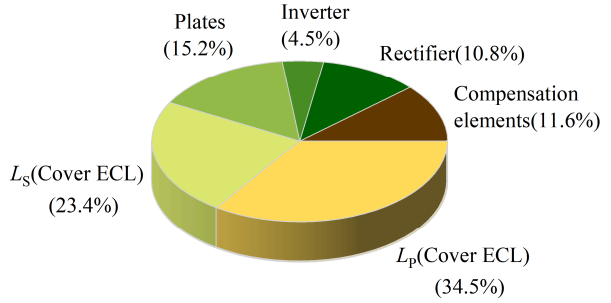


Fig. 17. The loss distribution of the UHWPT system.

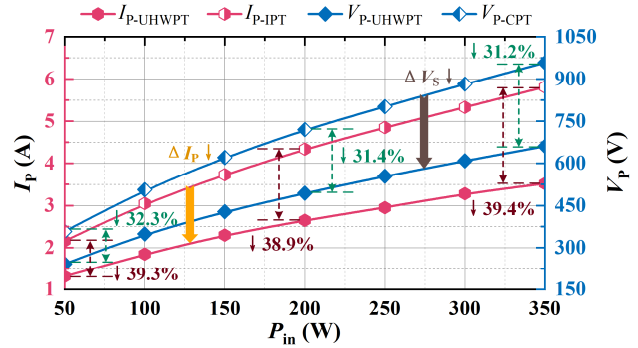


Fig. 18. Comparison of the UHWPT system to the UIPT and UCPT systems regarding coil current and SIP voltage.

As shown in Fig. 16, the load current I_R is independent of the load R_L and remains at approximately 2.2 A, indicating that the proposed system exhibits the load-independent CC output characteristic. With the load ranging from 40 to 70 Ω , the system efficiency remains above 85%. In particular, the dc-dc efficiency reaches the maximum value at 87.8% when the load resistance is 50 Ω , and the input power is 278 W. The experimental system's power loss is 34W, primarily including the loss from the coupler, inverter, rectifier, and compensation elements. According to the experimental measurement and calculation, the loss distribution of the UHWPT system is shown in Fig. 17, with the significant loss occurring in the ECL caused by the transmitter and receiver coil currents.

C. Comparison with Single UIPT and UCPT Systems

The proposed system is compared with the SS-compensated UIPT and UCPT systems to validate the ability to reduce the ECL by decreasing the coil currents and suppress the SIP voltage stresses. Fig. 18 shows the variation of I_P and V_P with input power P_{in} , in which $I_P-UHWPT$ and $V_P-UHWPT$ represent the coil current and the SIP voltage of the proposed UHWPT system. At the same time, I_P-UIPT and V_P-UCPT correspond to the coil current and the SIP voltage of the UIPT and UCPT systems, respectively. When the input power P_{in} is 50 W, 200 W, and 350 W, $I_P-UHWPT$ is 39.3%, 38.9%, and 39.4% lower than I_P-UIPT , respectively. Similarly, $V_P-UHWPT$ is 32.3%, 31.4%, and 31.2% lower than V_P-UCPT , respectively. Thus, compared to the SS-compensated UIPT and UCPT systems at the same input power, the average suppression of the coil currents and the SIP voltage stresses of the proposed system is improved

> IEEE Transactions on Power Electronics <

TABLE II
COMPREHENSIVE COMPARISON BETWEEN DIFFERENT WORKS

Reference	System	Frequency	Power	Compensation topology	Efficiency	SIP voltage	Test condition
[9]	UIPT	337 kHz	158 W	SS	80%	No	Seawater
[10]	UIPT	523.9 kHz	194 W	SS (two transmitter coils)	82%	No	Seawater
[11]	UIPT	504.5 kHz	200 W	SS	85%	No	Seawater
[8]	UCPT	107.7 MHz	400 W	SS	90%	N/A	Freshwater
[16]	CPT	800 kHz	2039 W	LC-CLC	90.29%	3791 V	Air
[17]	CPT	500 kHz	40 W	LCLC-LCLC	83%	1030 V	Air
This work	UHWPT	800 kHz	278 W	LC-LC	87.8%	576 V	Seawater

respectively by 39.1% and 31.3%. It is indicated that both the ECL caused by the coil currents and the plate voltage stresses are significantly reduced.

Table II lists a comprehensive comparison with respect to the existing literature studies. Compared with the coupler in [10], this paper proposes a more compact integrated magnetic-electric coupler suitable for the UHWPT system without adding additional transmitter coils, reducing the system size. In [8], although the efficiency reaches the value of 90%, the working frequency is much higher than this work, increasing the difficulty of the overall system design. Compared with [9], [10], [11] and [17], the proposed system has better transfer efficiency. Compared with [16] and [17], the proposed system does not need to design complex high-order compensation networks to optimize the plate voltage stresses, and the parameter design process is simpler.

Therefore, this paper provides a novel and adaptable solution for efficient and safe underwater wireless power transfer by drawing on previous work and incorporating the HWPT technology. However, the insulation isolation between the same side plates and coils in the integrated magnetic-electric coupler is an important issue to be considered in the application. In the future, the coupler will be designed to quantitatively analyze the gap between the plates and the coils and take targeted insulation measures.

VI. CONCLUSION

This paper proposes a novel UHWPT system to achieve high-efficiency and low plate voltage stresses. The magnetic and electric field coupling energy transfer channels of the integrated coupler can be compensated for each other. The ECL caused by the coil currents as well as the voltage stresses among the coupling plates can be significantly reduced by rationally allocating the power of the two types of transfer channels. With the FHA method, the system's working principle is analyzed to derive the expression of the power ratio. Then, combining the impact of geometric dimensions and insulation on the coupler parameters, a design method of the system based on the double

optimization parameters is proposed. Experimental results show that the proposed UHWPT system achieves the load-independent CC output with a maximum efficiency of 87.8%. The average suppression of the coil currents and SIP voltage stresses is improved by 39.1% and 31.3% compared to the SS-compensated UIPT and UCPT systems at the same power, respectively.

REFERENCES

- [1] Y. Wang, T. Li, M. Zeng, J. Mai, P. Gu, and D. Xu, "An Underwater Simultaneous Wireless Power and Data Transfer System for AUV With High-Rate Full-Duplex Communication," *IEEE Trans. Power Electron.*, vol. 38, no. 1, pp. 619-633, 2023.
- [2] A. Mostafa, Y. Wang, S. Tangirala, H. Zhang, and F. Lu, "A 5 kW Hull-Compatible Inductive Charging System With 360° Folded Spatial Unipolar Coupler for Autonomous Underwater Vehicles (AUVs)," *IEEE Trans. Ind. Appl.*, vol. 59, no. 6, pp. 7001-7012, 2023.
- [3] S. Pang, J. Xu, H. Li, Q. Ma, and X. Li, "Dual-Frequency Modulation to Achieve Power Independent Regulation for Dual-Load Underwater Wireless Power Connector," *IEEE J. Emerging Sel. Top. Power Electron.*, vol. 11, no. 2, pp. 2377-2389, 2023.
- [4] Z. Zhang, H. Pang, A. Georgiadis, and C. Cecati, "Wireless Power Transfer—An Overview," *IEEE Trans. Ind. Electron.*, vol. 66, no. 2, pp. 1044-1058, 2019.
- [5] F. Wang, Q. Yang, X. Zhang, Z. Yuan, and X. Ni, "Optimizing Levitation Devices for Wireless Power Transfer: An Fe-NCS Grid Structure Approach," *IEEE Trans. Power Electron.*, vol. 38, no. 10, pp. 11859-11869, 2023.
- [6] L. Yang, X. Li, Y. Zhang, B. Feng, T. Yang, H. Wen, J. Tian, D. Zhu, J. Huang, A. Zhang, and X. Tong, "A review of underwater inductive wireless power transfer system," *IET Power Electron.*, vol. no. pp. 2023.
- [7] C. R. Teeneti, T. T. Truscott, D. N. Beal, and Z. Pantic, "Review of Wireless Charging Systems for Autonomous Underwater Vehicles," *IEEE J. Oceanic Eng.*, vol. 46, no. 1, pp. 68-87, 2021.
- [8] M. Tamura, Y. Naka, K. Murai, and T. Nakata, "Design of a Capacitive Wireless Power Transfer System for Operation in Fresh Water," *IEEE Trans. Microwave Theory Tech.*, vol. 66, no. 12, pp. 5873-5884, 2018.
- [9] K. Zhang, Y. Ma, Z. Yan, Z. Di, B. Song, and A. P. Hu, "Eddy Current Loss and Detuning Effect of Seawater on Wireless Power Transfer," *IEEE J. Emerging Sel. Top. Power Electron.*, vol. 8, no. 1, pp. 909-917, 2020.
- [10] K. Zhang, X. Zhang, Z. Zhu, Z. Yan, B. Song, and C. C. Mi, "A New Coil Structure to Reduce Eddy Current Loss of WPT Systems for Underwater Vehicles," *IEEE Trans. Veh. Technol.*, vol. 68, no. 1, pp. 245-253, 2019.
- [11] Z. Yan, Y. Zhang, T. Kan, F. Lu, K. Zhang, B. Song, and C. C. Mi, "Frequency Optimization of a Loosely Coupled Underwater Wireless Power Transfer System Considering Eddy Current Loss," *IEEE Trans. Ind. Electron.*, vol. 66, no. 5, pp. 3468-3476, 2019.
- [12] T. Chen, C. Cheng, H. Cheng, C. Wang, and C. C. Mi, "Load-Independent

> IEEE Transactions on Power Electronics <

- Power-Repeater Capacitive Power Transfer System With Multiple Constant Voltage Outputs," *IEEE J. Emerging Sel. Top. Power Electron.*, vol. 10, no. 5, pp. 6358-6370, 2022.
- [13] T. Chen, C. Cheng, H. Cheng, C. Wang, and C. C. Mi, "A Multi-Load Capacitive Power Relay System With Load-Independent Constant Current Outputs," *IEEE Trans. Power Electron.*, vol. 37, no. 5, pp. 6144-6155, 2022.
- [14] R. Mai, B. Luo, Y. Chen, and Z. He, "Double-sided CL compensation topology based component voltage stress optimisation method for capacitive power transfer charging system," *IET Power Electron.*, vol. 11, no. 7, pp. 1153-1160, 2018.
- [15] J. Lian, and X. Qu, "Design of a Double-Sided LC Compensated Capacitive Power Transfer System With Capacitor Voltage Stress Optimization," *IEEE Trans. Circuits Syst. II Express Briefs*, vol. 67, no. 4, pp. 715-719, 2020.
- [16] B. Luo, A. P. Hu, H. Munir, Q. Zhu, R. Mai, and Z. He, "Compensation Network Design of CPT Systems for Achieving Maximum Power Transfer Under Coupling Voltage Constraints," *IEEE J. Emerging Sel. Top. Power Electron.*, vol. 10, no. 1, pp. 138-148, 2022.
- [17] J. Lian, X. Qu, X. Chen, and C. C. Mi, "Design of a Double-Sided LCLC-Compensated Capacitive Power Transfer System With Predesigned Coupler Plate Voltage Stresses," *IEEE J. Emerging Sel. Top. Power Electron.*, vol. 10, no. 1, pp. 128-137, 2022.
- [18] H. Zhang, and F. Lu, "Insulated Coupler Structure Design for the Long-Distance Freshwater Capacitive Power Transfer," *IEEE Trans. Ind. Inf.*, vol. 16, no. 8, pp. 5191-5201, 2020.
- [19] M. Tamura, K. Murai, and M. Matsumoto, "Design of Conductive Coupler for Underwater Wireless Power and Data Transfer," *IEEE Trans. Microwave Theory Tech.*, vol. 69, no. 1, pp. 1161-1175, 2021.
- [20] B. Luo, T. Long, L. Guo, R. Dai, R. Mai, and Z. He, "Analysis and Design of Inductive and Capacitive Hybrid Wireless Power Transfer System for Railway Application," *IEEE Trans. Ind. Appl.*, vol. 56, no. 3, pp. 3034-3042, 2020.
- [21] F. Lu, H. Zhang, H. Hofmann, and C. C. Mi, "An Inductive and Capacitive Combined Wireless Power Transfer System With LC-Compensated Topology," *IEEE Trans. Power Electron.*, vol. 31, no. 12, pp. 8471-8482, 2016.
- [22] F. Lu, H. Zhang, H. Hofmann, and C. C. Mi, "An Inductive and Capacitive Integrated Coupler and Its LCL Compensation Circuit Design for Wireless Power Transfer," *IEEE Trans. Ind. Appl.*, vol. 53, no. 5, pp. 4903-4913, 2017.
- [23] X. Li, C. Tang, X. Dai, P. Deng, and Y. Su, "An Inductive and Capacitive Combined Parallel Transmission of Power and Data for Wireless Power Transfer Systems," *IEEE Trans. Power Electron.*, vol. 33, no. 6, pp. 4980-4991, 2018.
- [24] X. Qing, Z. Li, X. Wu, Z. Liu, L. Zhao, and Y. Su, "A Hybrid Wireless Power Transfer System With Constant and Enhanced Current Output Against Load Variation and Coupling Misalignment," *IEEE Trans. Power Electron.*, vol. 38, no. 10, pp. 13219-13230, 2023.
- [25] P. Chen, J. Liu, H. Zhang, and B. Chu, "Increase of capacitance of thick dielectrics by fringe effect," *IEEE Trans. Dielectr. Electr. Insul.*, vol. 26, no. 5, pp. 1716-1719, 2019.
- [26] H. Zhang, F. Lu, H. Hofmann, W. Liu, and C. C. Mi, "A Four-Plate Compact Capacitive Coupler Design and LCL-Compensated Topology for Capacitive Power Transfer in Electric Vehicle Charging Application," *IEEE Trans. Power Electron.*, vol. 31, no. 12, pp. 8541-8551, 2016.
- [27] C. Rong, X. Tao, C. Lu, and M. Liu, "Investigation of Magnetic Field Shielding by Mesh Aluminum Sheet in Wireless Power Transfer System," in *Proc. IEEE Wireless Power Transfer Conf.*, London, UK, Jun. 2019, pp.126-129.
- [28] F. Xu, and H. Huang, "Frequency selection for underwater wireless power transfer based on the analysis of eddy current loss," *AEU Int. J. Electron. Commun.*, vol. 163, no. pp. 154618, 2023.



Xian Zhang received the M.E., and Ph.D. degrees in electrical engineering from the Hebei University of Technology, Tianjin, China, in 2009, and 2012, respectively.

He is currently a Professor with the Hebei University of Technology, Tianjin, China. He is the director of the China Electrotechnical Society and the secretary-general of the National Specialized Committee on Wireless Power Transmission Technology.

His research interests encompass intelligent high-power wireless power transmission technology, measurement of three-dimensional electromagnetic fields, and numerical calculations of modern engineering electromagnetic fields.



Guangyao Li received the B.S. degree in electrical engineering and intelligent control from the Tianjin Sino-German University of Applied Sciences, Tianjin, China, in 2022. He is currently working toward the M.E. degree in electrical engineering with the Hebei University of Technology, Tianjin, China.

His research interests include engineering electromagnetism, wireless power transfer, and its industrial applications.



Ting Chen received the B.S., M.S., and Ph.D. degrees from the China University of Mining and Technology, Beijing, China, in 2015, 2017, and 2022, respectively. From November 2019 to November 2021, she was a joint Ph.D. student with the Department of Electrical and Computer Engineering, San Diego State University, San Diego, CA, USA.

She is currently an assistant professor with the Department of Electrical Engineering and State Key Laboratory of Reliability and Intelligence of Electrical Equipment, Hebei University of Technology.

Her current research interests include wireless power transfer technologies, modeling and control of switching converters.



Fengxian Wang received the B.S. degree in electrical engineering and the M.S. degree in electrical engineering from Tiangong University, Tianjin, China, in 2018 and 2021, respectively. He is currently working toward the Ph.D. degree with the Hebei University of Technology, Tianjin, China.

His research interests include engineering electromagnetism, wireless power transfer, and its industrial applications.

> IEEE Transactions on Power Electronics <



Qingxin Yang received the B.S., M.S., and Ph.D. degrees from the Hebei University of Technology, Tianjin, China, in 1983, 1986, and 1997, respectively.

Since 1996, he has been a Professor with the Hebei University of Technology. From 2008 to 2018, he was the President of Tianjin Polytechnic University, China. From 2018 to 2020, he was the President of the Tianjin University of Technology, China. His research interests include computational electromagnetism, engineering electromagnetism and their applications, and special wireless power transfer.

Dr. Yang was a Board Member of International COMPUMAG Society and the President of China chapter. Since 2015, he has been the President of China Electrotechnical Society.



Weida Xu received the B.S. degree in electrical engineering and automation from the Hebei Agricultural University, Hebei, China, in 2021. He is currently working toward the M.E. degree in electrical engineering with the Hebei University of Technology, Tianjin, China.

His research interests include engineering electromagnetism, wireless power transfer, and its industrial applications.